Gravity effects on fines migration in sandstone: A numerical approach in 3D with complete forces set

Shitao Liu, *Igor* Shikhov, and *Christoph* Arns*

School of Minerals and Energy Resources Engineering, University of New South Wales, Sydney, Australia

Abstract. One of the most significant and least understood aspects of fines motion in rocks is the process of clogging, which can occur even when fines smaller than a critical throat diameter are mobilized. Pore clogging dynamics is defined by interactions acting across vastly different scales: from pore-scale transport to colloid-scale mechanical and hydraulic interactions, and the sub-colloid scale at which electrochemical interactions occur. So far numerical models for pore clogging dynamics including all acting forces have been limited to 2D representations of rock samples. In this work a coupled fines tracking approach combining computational fluid dynamics (CFD) and a discrete element model (DEM) is utilized to predict fines retention and pore clogging, including surface forces and gravity effects associated with density differences between fines and the saturating brine. A dynamically adaptive CFD mesh is automatically refined around particles to resolve the fine-scale fluid flow around fines. Furthermore, particle trajectories are recorded and related to individual pores and throats of the rock sample. Here we carry out calculations on a digital representation of Bentheimer sandstone and focus on particle density as a main factor. For the fines with higher density, the spatial change of particle trapping suggests that gravity tends to facilitate the transport of fines in the direction of gravity but impedes their transport along the flow direction. Given fines of different densities, we quantify the effects of gravity on particle trajectories, which indicates that the denser fines can traverse further along the flow direction due to two mechanisms: passage through gravitationally downward throats and modification of flow pathways induced by pore clogging.

1 Introduction

The transport and retention of fine particles in porous media is a phenomenon of immense significance to a multitude of industrial or environmental applications including enhanced oil recovery (EOR) and reservoir protection [1, 2], carbon capture and storage (CCS) [3], spread of bacterial pathogens within groundwater reservoirs [4, 5], and wastewater treatment by granular filtration [6, 7]. In the petroleum industry, alterations in the physicochemical environment can mobilize fine particles, triggering their migration during water flood operations with subsequent fines retention at throats. The latter is widely acknowledged as a primary mechanism of formation damage, causing significant impairment in reservoir permeability and well productivity [8].

The complexity of fines transport dynamics is attributed to phenomena and interactions spanning different scales. These encompass pore-scale transport, particle-scale interactions, and subcolloid-scale electrochemical surface interactions. As a result, fines transport dynamics are comprehensively governed by a variety of physical and chemical factors, including particle size [9, 10], pore morphology [11, 12], surface roughness [13, 14], ionic strength [15, 16], flow rate [17, 18], and gravitational force [19, 20]. Gravity plays a pivotal role in influencing the dynamics of fines, including their detachment from solid surfaces, movement within the flow domain, and deposition, by significantly contributing to the determination of the fines' equilibrium state [20]. Liu et al. [21] conducted migration studies involving neutrally buoyant latex and non-buoyant glass microspheres within microfluidic devices comprised of cylindrical columns. They noted that the glass particles showed enhanced retention on the bottom substrate of the porous matrix. Wan et al. [22] executed a theoretical and experimental assessment of bacterial sedimentation within sand packs under hydrostatic conditions. Their findings affirmed that gravitational force can significantly boost downward transport within a porous medium, suggesting that sedimentation could serve as a critical retention mechanism. Within the filtration experiments using kaolinite and montmorillonite fines within a saturated glass bead pack, Chrysikopoulos et al. [19] observed more pronounced particle retention in up-flow scenarios (flow direction opposes gravity) as compared to down-flow cases (flow direction aligns with gravity). Further investigations are still necessary to comprehend the impact of gravity on fines' trajectories at the pore scale within natural porous media, particularly in materials resembling reservoir rocks. The complex pore structure of rocks fosters intricate fines transport and retention dynamics. For example, in sandstone, the correlation

* Corresponding author: c.arns@unsw.edu.au

between flow velocity and shear rate exhibits a broader range than what is typically observed in sphere packs or tube bundles [23]. Moreover, the broader pore and throat size distributions in sandstone ensure that multiple mechanisms of particle retention including size exclusion, bridging, surface attachment, and both deposition and accumulation, are relevant. Gravity, by directing fines gravitationally downwards, adds another layer of intricacy to fine particle transport within rocks, causing it to deviate from the fluid-propelled trajectory. These complexities render the prediction of fines transport and retention within reservoir rocks a challenging task.

Computational fluid dynamics (CFD) coupled with the discrete element method (DEM), known as the CFD-DEM approach, offers a powerful tool for simulating the trajectories and movement of particles by computing the resultant force acting on each particle, derived from local fluid flow effects. This multi-scale Eulerian-Lagrangian method considers individual particles as discrete entities, and the fluid phase as a continuum. Mirabolghasemi et al. [24] proposed an innovative CFD-DEM modeling approach to predict fine particle retention with sandstone and sphere pack structures in 3D by utilizing the X-ray microtomography as a mean to construct the geometric input for the flow domain. In their work, due to the relatively large particle size and density employed, particles were retained by physical mechanisms of straining and bridging. The electrostatic surface attachment was not considered in their filtration system. For computational efficiency, fluid flow calculations were not coupled with particle motion. Elrahmani et al. [25] utilized a fine CFD mesh where the cells are several times smaller than the simulated particles to resolve the effects of particle retention on fluid flow field. They investigated pore clogging phenomena caused by the physical retention mechanisms within a 2D sand pack geometry extracted using computed tomography. Kermani et al. [26] integrated the DEM with the Lattice Boltzmann Method (LBM) to explore the influence of superficial fluid velocity and particle size on colloid retention and detachment. Up to this point, numerical models addressing fines transport including all acting forces have primarily been confined to 2D representations. While 2D models offer valuable insights, they can oversimplify complex three-dimensional interactions and spatial configurations, potentially limiting their accuracy and predictive power for realistic scenarios.

In this study we proposed a resolved CFD-DEM modeling approach with the complete force set, including hydraulic interaction, electrostatic surface interaction, mechanical collision, buoyancy, and gravity, to investigate the gravity effects on fines transport in a Bentheimer sandstone sample. The flow domain and solid grain surfaces are extracted from segmented X-ray microtomography, and this proposed model is adaptable to any porous media provided that 3D images are available. We explore the particle retention distribution in relation to gravity and flow directions within the sandstone sample considering different fine densities. Following this, we examine the deviation in trajectories caused by gravity compared to neutrally buoyant fines. Ultimately, we analyze transport within specific pores and throats to examine the unexpected transport behavior that a portion of the denser fines demonstrates: a limited transport along the gravity direction and extended transport along the flow direction compared to the neutrally buoyant fines.

2 Methodology

The objective of this study is to evaluate the gravity effects on fines transport and retention within sandstone, which requires the inclusion of interactions acting on fines at different scales ranging from sub-particle-scale electrochemical interactions to pore-scale transport. In subsequent sections, we first introduce the approach for CFD-DEM modeling including fines motion calculations, fluid flow simulations, and particle-fluid coupling. This is succeeded by an exposition of the model setup.

2.1 CFD-DEM modeling

A complete force set that includes mechanical contact forces, electrostatic surface forces, hydrodynamic forces, gravity, and buoyancy, is considered in this study. The velocity of the objective particle *i*, which may potentially collide with another particle *j* or/and the solid grain *k*, is determined by solving the following translation and rotation motion equations:

$$m(i)\frac{d\boldsymbol{v}(i)}{dt} = \sum_{N} F_c^n(i,j) + \sum_{N} F_c^t(i,j) + \sum_{N} F_S(i,j) + F_c^n(i,k) + F_c^t(i,k) + F_u(i) + F_l(i) + F_g(i), \quad (1)$$

$$\frac{dI(i)\omega(i)}{dt} = \sum_{N} r_{ic} \times F_c^t(i,j) + r_{ic} \times F_f(i,k), \quad (2)$$

where $\boldsymbol{v}$ and m are particle velocity and mass. N is the number of particles that impose a force (either contact force or surface force) on the target particle at a simulated time t. F_c^n and F_c^t are the normal and tangential contact forces caused by collisions. F_S, F_u, F_l and F_g are electrostatic surface forces, drag, buoyancy, and gravity acting on the particle *i*, respectively. Considering the relatively large particle size and high flow velocity employed in our filtration system, diffusion effects on fines are not incorporated in this study [27]. The contact forces exerted on particles due to collisions are approximated by the spring-dashpot model [28] which decomposed the colliding forces in two parts: the rebound of the particles in contact and the energy losses which is caused by the damping mechanism. The approach to incorporate the particle-solid surface interactions into the tracking model follows the method outlined by Liu et al. [11]. The interparticle surface interaction is evaluated using DLVO theory, which accounts for the net potential originating from both electrostatic repulsion and van der Waals attraction at the relevant separation distance. The electrostatic interaction is represented by the screened Coulomb repulsion, also known as Yukawa potential [29]. The van der Waals potential between two spherical colloidal particles is determined based on the method

presented in the study by Hamaker [30]. The fluid flow is simulated by solving the Navier-Stokes equations of incompressible fluid flow within the discretized flow domain with the boundary and initial conditions. The fluid-particle coupling, which evaluates the influence of particle motion on fluid flow and the hydraulic forces exerted on particles, is accomplished based on the methodology suggested by Kloss et al. [31].

2.2 Model setup

In this study, fines transport and retention are simulated within Bentheimer sandstone. The flow domain for fines transport and the solid grain surface features are provided by an X-ray computed microtomography image. This micrographic image is segmented into a binary representation consisting of a solid phase and a void phase via an active contour method [32]. A surface mesh that is directly extracted from the outer surface of the solid phase in the segmented image is employed as the grain surface to constrain particle motion within the void space. The flow domain for fluid simulation is generated and discretized by the snappyHexMesh utility in OpenFOAM [33]. Firstly, a structured mesh composed of uniformly-sized hexahedral cells is created to encompass the entire calculation domain, including both the solid and pore regions. Next, the hexahedral cells proximal to the grain surface boundary defined by the extracted grain surface mesh are split into smaller cells to enhance the local resolution near the solid-pore interface. Subsequently, the cells situated within the solid phase region are discarded. The resulting mesh that characterizes the pore space is prepared for fluid flow simulations and the coupling between particle and fluid phases.

The flow domain for fines transport is chosen as a subdomain of the three-dimensional digital image that comprises 400 ×500 ×500 voxels at a resolution of 2.15 μm/voxel. In order to examine the impact of gravity on particle transport and retention, the flow direction of fluid is oriented perpendicular to the direction of gravity. A free-flow region is introduced before the porous matrix region in the flow direction, which assists to establish the realistic flow field and determine the particle injection velocity at the entrance surface of the sandstone. In the flow simulation, no-slip boundary conditions are imposed at the solid surface and the Y and Z bounding surfaces.
To minimize the impact of the truncated boundaries, the region where the normal distance to the Y or Z bounding surfaces is smaller than the length of 50 voxels is excluded for particle injection (see Fig. 1). Also, fines retained within this bounding region are excluded from subsequent data analysis. At the inlet surface, the truncated boundaries may cause unexpected retention when fines transition from non-porous regions into the porous matrix. This retention can potentially facilitate a mud cake on the injection surface, thereby resisting the invasion of fines into the porous region. To prevent the formation of filter cake at the entrance, particles are injected at the pore centers on the entry surface. Furthermore, such particle injection at the pore center also assists to mitigate the stochasticity arising from random particle injection positions and allows for a more focused examination of

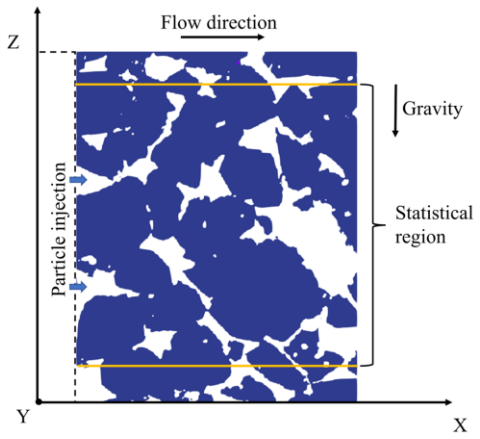

Fig. 1. Slice through the 3D simulation domain within Bentheimer sandstone. The fluid flow direction is perpendicular to the direction of gravity. The area between the yellow lines is the statistical region for particle injection and counting.

the effects of gravity on fines transport and retention. To accomplish this particle injection, the pore space at the entry surface is partitioned into individual pores by performing the watershed segmentation [34] (Fig. 2a). The position of the voxel with the largest distance value in each individual pore designates the pore center for the fines injection (Fig. 2b). We employed lattice Boltzmann method (LBM) [35] to derive the fluid velocity distribution on the entry surface (Fig. 2c). The D3Q19 lattice (3-dimensional lattice with 19 feasible velocity directions) [36] is selected. This calculated velocity field (Fig. 2c) is subsequently mapped to the labeled pore field to determine the fluid flux fraction of each pore. The rate of particle insertion into each pore is contingent upon the fluid flux of the respective pore. The particle retention at the pore-throat may result in a modification of fluid flow distribution within the sample, thereby altering the fluid flux and particle injection rate into each pore. To resolve the variations in particle mass flux on the entrance surface, the fluid flux and the corresponding particle injection rate are recalculated for every 0.5 pore volume of fluid injection. The adaptive local refinement technique employing the octree approach [37] is implemented to enhance the mesh resolution of particle-occupied regions. The cells occupied by particles are recursively subdivided into eight uniformly sized sub-cells until the newly generated cells achieve the desired resolution. In this study, an original mesh resolution of 7.5 μm/cell is utilized, and the cells encompassed by particles are subdivided two times to attain a finer local resolution of 1.875 μm/cell, satisfying the criterion of having eight cells per particle diameter [38].

Simulations are performed mimicking the filtration process of fine particles of 15 μm diameter flowing through the sandstone with a superficial fluid velocity of 0.001 m/s. Two study cases employing different particle densities of 1000 kg/m^3 and 2000 kg/m^3 are conducted to explore the gravity effects. In each case, two pore volumes of particle suspension with a particle volumetric concentration of 0.5% are injected. Following the particle injection, the sandstone is flushed with the fluid without particles until all particles complete their motion within the sandstone or flow out of the filtration system.

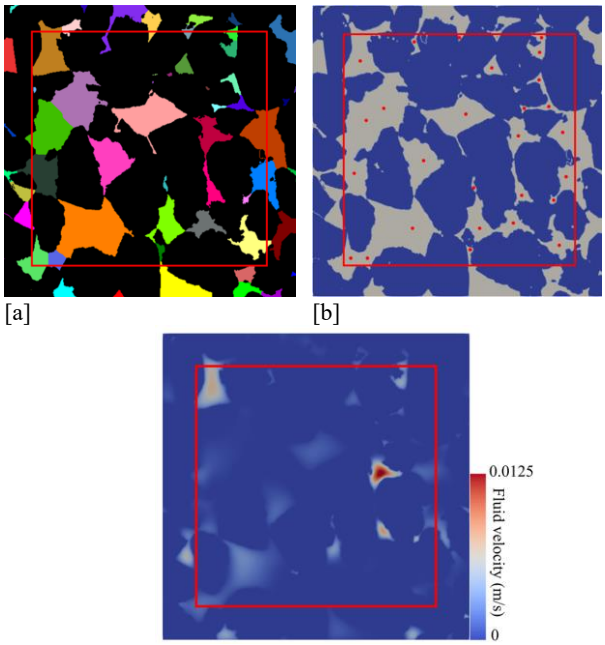

Fig. 2. [a] The watershed pore partitioning results of the entry surface slice (through the fluid flow direction). The red rectangle represents the objective region for particle injection and trajectory analysis. [b] Visualization of the centers of each individual pore. [c] LBM-calculated fluid velocity distribution on the entry surface.

Table 1. Parameters used in the fines tracking simulations.

	Value	Unit
Solid phase		
Particle diameter	15	μm
Particle density	1000 and 2000	kg/m^3
Restitution coefficient	0.9	-
Grain Young's modulus	70	GPa
Particle Young's modulus	20	MPa
Grain Poisson's ratio	0.3	-
Colloid Poisson's ratio	0.3	-
Friction factor	0.15	-
Liquid phase		
Liquid density	1000	kg/m^3
Liquid viscosity	1×10^{-3}	$Pa{\cdot}s$
Superficial velocity	0.00025	m/s
Simulation time step		
DEM time step	1×10^{-7}	s
CFD time step	3×10^{-6}	s
Coupling interval	30	-

Favorable particle attachment conditions under an ionic strength of 300 *mM* are chosen in this study. The particle surface potential is selected as the one of polystyrene particles reported by Tufenkji and Elimelech [39]. We employ the quartz sand surface potential of Leroy et al. [40]. Some parameters necessary for simulating a realistic filtration system, including the particle surface restitution coefficient, Young's modulus, the DEM and CFD time steps, and the coupling interval, are determined based on the colloid tracking modeling proposed by Liu et al. [11] The final set of properties and parameters utilized in this particle tracking modeling is summarized in Table 1.

3 Results

In this section, we compare the spatial distributions for two study cases with differing particle densities within the Bentheimer sandstone. Subsequently, we assess the deviation in trajectories between these two cases, which arise from differential gravitational forces imposed on the fines. Finally, we scrutinize the impact of the gravity-induced trajectory deviations on the evolution of fluid flux (or permeability) within a specific throat.

3.1 Spatial distribution of retained fines

We present the spatial distributions of retained fines for two filtration cases: one where the particle density equals that of water, and the other where the particle density is twice that of water. This serves as a preliminary demonstration of gravity's impact on fine particle transport within a complex flow domain. In order to investigate the spatial distribution of retained fines along gravitational direction and flow directions, we partitioned the flow domain space of the rock into ten parallel sections of equal thickness (50 voxels), according to direction of interest (X and Z direction). Following this, we count the number of retained fines within each segment.

Fig. 3a demonstrates the distribution of retained fines along the gravitational direction. It can be observed that in segments 1 and 2 (the bottommost segments of the sample), a larger quantity of fines is retained in the scenario where particle density is higher. Conversely, in the uppermost region (segment 8), a higher accumulation of neutrally buoyant fines is detected. The pattern of fines retention distribution in the top and bottom regions confirms expectations that gravity promotes a downward transport of fines. In the flow direction, the vast majority of fines of both density types are captured within the first half of the sample (segments 1 to 4), Fig. 3b. This limited transport distance can be attributed to the favorable attachment conditions operative in this study. Under a relatively high ionic strength, the abundant ion concentration can effectively screen the double-layer repulsion between fines and solid surface. As a result, the attractive van der Waals forces become dominant within the electrostatic surface interactions and lead to a immediate fines retention after collisions. The complex geometry of the flow domain contributes to the frequent fines-grain contacts, which subsequently leads to immediate fines retention due to the resultant surface forces. Moreover, the retained fines alter original grain surfaces, increasing likelihood of capturing incoming fines due to inter-particle surface interactions, effectively serving as additional collectors. As per the cumulative retention profiles depicted in Fig. 3b, the lower retention of neutrally buoyant fines within the first two segments, adjacent to the inlet, hints at their better transport capability, as they closely follow fluid flow streamlines. As for the denser fines, gravity deviates their trajectories from local streamlines, which increases the probability of fines-solid collisions or deposition, consequently impeding their transport along with the carrier fluid.

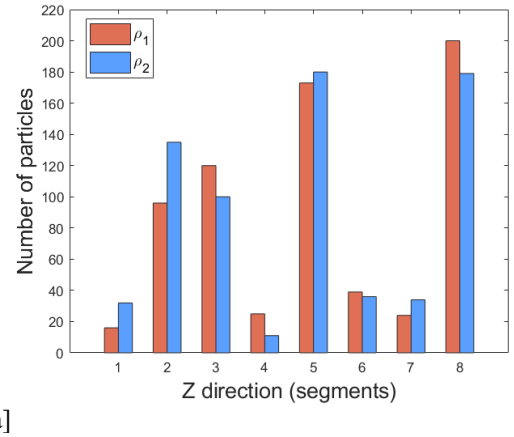

[a]

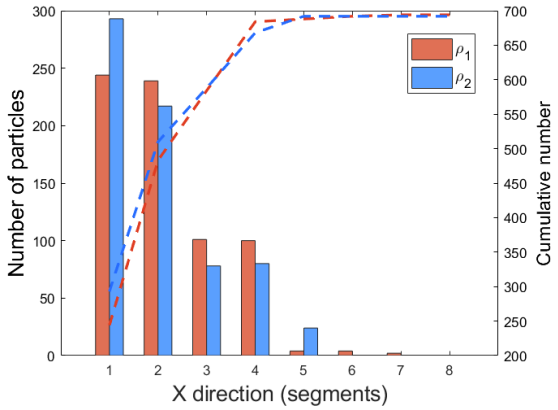

[b]

Fig. 3. The spatial distribution of fines retention along the gravitational direction [a] and the flow direction [b] within the sandstone sample. It should be noted that segments 1 through 8 in the gravitational direction are vertically arranged from the bottom to the top of the sample, while segments 1 through 8 in the flow direction are arranged from the flow inlet to the outlet. ρ_1 and ρ_2 refer to the two study cases corresponding to particle densities of 1000 kg/m^3 and 2000 kg/m^3, respectively.

3.2 Fines trajectory deviation

In this section, the influence of gravity on the fines transport trajectories is quantitatively investigated by comparing the trajectories of neutrally buoyant fines with those of denser fines possessing a density twice that of water. The fines injection rate in each segmented pore within the entrance surface (refer to Fig. 1) undergoes recalculation for every 0.5 pore volume (PV) injection, thus accommodating the influence of fines retention on the fluid flux distribution at the entrance surface. During each 0.5 PV injection, two particles that are injected into the same pore in identical order within the two cases are considered as a pair of concurrent particles. Trajectory deviations between the cases are calculated as the positional difference in the gravity and flow directions between the retained positions of each pair of concurrent fines. This process is achieved by subtracting the coordinates of the neutrally buoyant fines from those of the denser fines, as depicted in Fig. 4. In this analysis, it is important to note that if one particle from any pair of concurrent fines is found within the excluded boundary region, that particular pair is omitted from the trajectory deviation analysis.

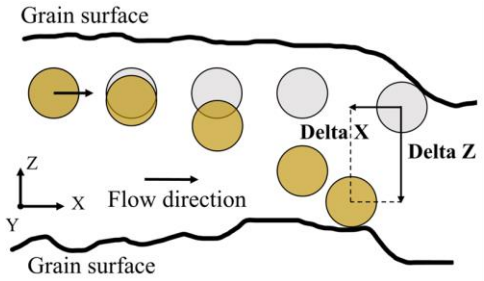

Fig. 4. A schematic demonstrating the calculation of trajectory deviation for two fines experiencing different gravitational forces. The gray and yellow spheres represent fines in the cases where the particle density is equal to and greater than that of the suspending fluid, respectively. Trajectory deviation is quantified as the positional difference between the retained positions of the concurrent particles in the flow and gravity directions, referred to as *Delta X* and *Delta Z*, respectively.

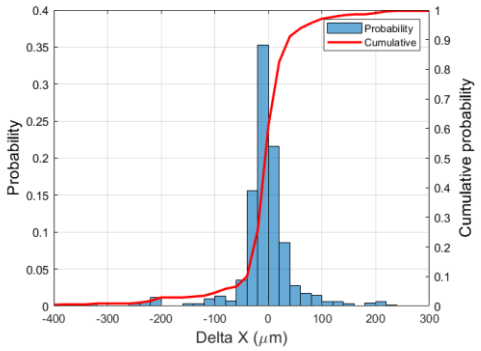

[a]

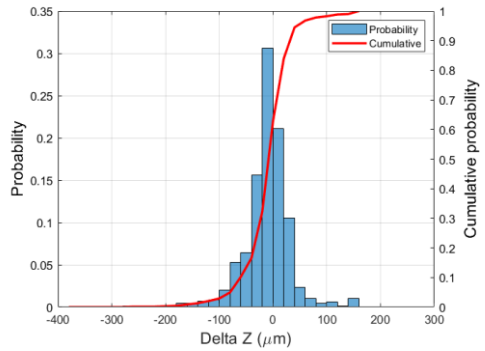

[b]

Fig. 5. The distribution corresponding to the trajectory deviations of fines between the two study cases wherein the particle density in one case is equivalent to that of the suspending fluid and twice that amount in the other case. These deviations are shown in the gravitational direction [a] and the flow direction [b].

Gravity can induce a deviation in the trajectories of fines from the local streamlines and promote gravitationally downward transport. This deviation can also prompt deposition on grain surface, leading to earlier retention compared to neutrally buoyant fines and resisting fines' transport with fluid flow. Consequently, denser fines are expected to traverse a longer distance in the gravity direction and a shorter distance along the flow direction. Nevertheless, Fig. 5a reveals that 37.2% of the denser fines still travel shorter distances along the gravity direction, while Fig. 5b indicates that 39.1% of them traverse a longer distance in the flow direction. This

discrepancy from the expectation can be attributed to two distinct mechanisms. Firstly, in the context of gravitationally downward throats, the fluid flow tends to converge at the throat entrance, often associated with a sudden change in flow direction. For neutrally buoyant fines, this abrupt shift can result in colliding of fines with the grain surface, leading to subsequent retention. Conversely, for denser fines, gravity can facilitate their passage through such downward throats, enabling their further transport with the fluid flow. The second mechanism occurs when denser fines flow into the downward throat under the influence of gravity but become trapped there. The continuous retention of fines eventually leads to the clogging of the downward throat. As a consequence, fluid flow is rerouted through other channels. This redirection of fluid flow, in turn, modifies the path of denser fines, enabling them to travel via these alternative channels, thereby avoiding entrapment in the downward throat. In our fines filtration simulations, the instances of fines transport behaviors corresponding to these two mechanisms described above are illustrated as follows.

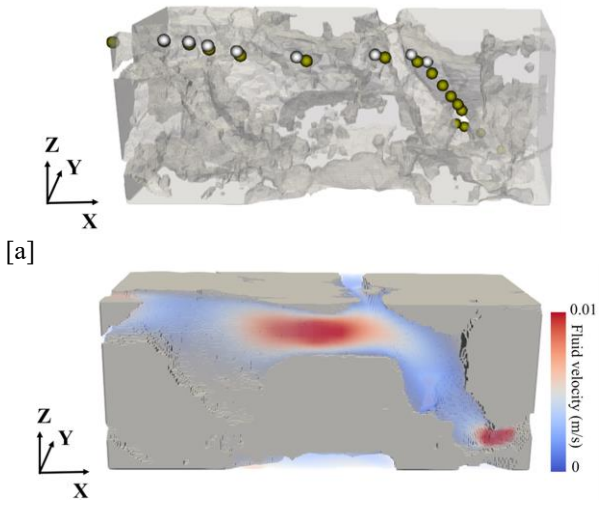

Fig. 6. [a] Trajectory comparison between a pair of concurrent fines. The color gray and yellow represent the neutrally buoyant particle and the denser particle, respectively. Spheres with the same color represent the trajectory of a single particle, with their positions recorded at regular time intervals. The grain phase is partially transparent to show the fines positions behind the grains. [b] Fluid velocity field within the shown pore space prior to the invasion of fines into the porous matrix.

Fig. 6 shows a scenario where gravity contributes to the passage of denser fines through a downward throat, resulting in a greater transport distance compared to neutrally buoyant fines. Fig. 6a displays the trajectories of a pair of concurrent fines, which shows the neutrally buoyant particle is intercepted by the top surface of the downward throat at the throat's entrance. In contrast, the denser particle influenced by gravity enters the throat with a lower trajectory in the *Z* direction and successfully passes through the downward throat, traveling a longer distance in the direction of flow. The local fluid velocity field is shown in Fig. 6b.

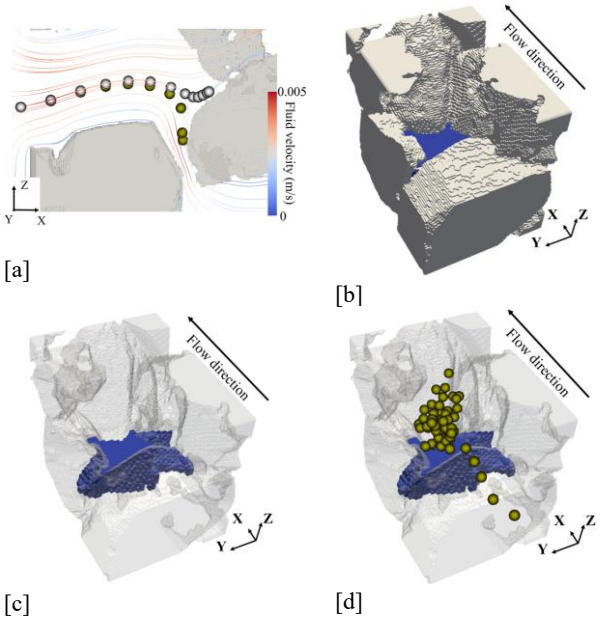

Fig. 7. [a] Trajectory comparison between the first injected pair of concurrent fines. Spheres with the same color represent the trajectory of a single particle, with their positions recorded at regular time intervals. Fluid streamlines have been generated from a 2D slice of the fluid field prior to the invasion of fines into the porous matrix. [b] A 3D visualization of the geometry of the gravitational downward throat shown in [a]. [c] A 3D visualization of the downward throat with a transparent grain phase, enabling a clear view of the throat geometry. [d] Snapshot of the accumulation of the denser fines at the downward throat.

Fig. 7 and Fig. 8 illustrate an alternative scenario where denser fines cause clogging in the downward throat, thereby redirecting fluid flow and leading to fines traversing alternate channels. The streamlines in Fig. 7a show the bifurcation of fluid flow into gravitationally upward and downward directions. The different trajectories of the first injected pair of fines at the bifurcation point (Fig. 7a) reveal the influence of gravity. The neutrally buoyant particle more closely follows the streamlines and tends to move upward. In comparison, the denser particle gravitates towards the downward pathway. This observation aligns with the findings of a study conducted by Chrysikopoulos [41], which simulated the transport of colloids within a bifurcation fracture system. The study reported that denser colloids preferentially gravitate towards the downward fracture. The retained dense particle within the throat constricts the available space for fluid flow. This constraint potentially alters the ability of local pores or throats to facilitate fluid passage. To explore the alteration of fluid flow caused by the retained fines, the temporal evolution of fluid flux of the downward throat (Fig. 7b) is investigated in the two filtration cases with various fines densities. Fig. 7c reveals the geometry of the downward throat by rendering the grain phase partially transparent. Fig. 7d further illustrates the throat geometry by showing with the aggregation of denser fines to demonstrate the way that the fines accumulate near the given throat. It should be noted that the fines retained inside the throat are not visible in Fig. 7d. Subsequently, the deviation in flux profiles in the two filtration cases is illustrated by the corresponding configuration of the retained fines and the local fluid

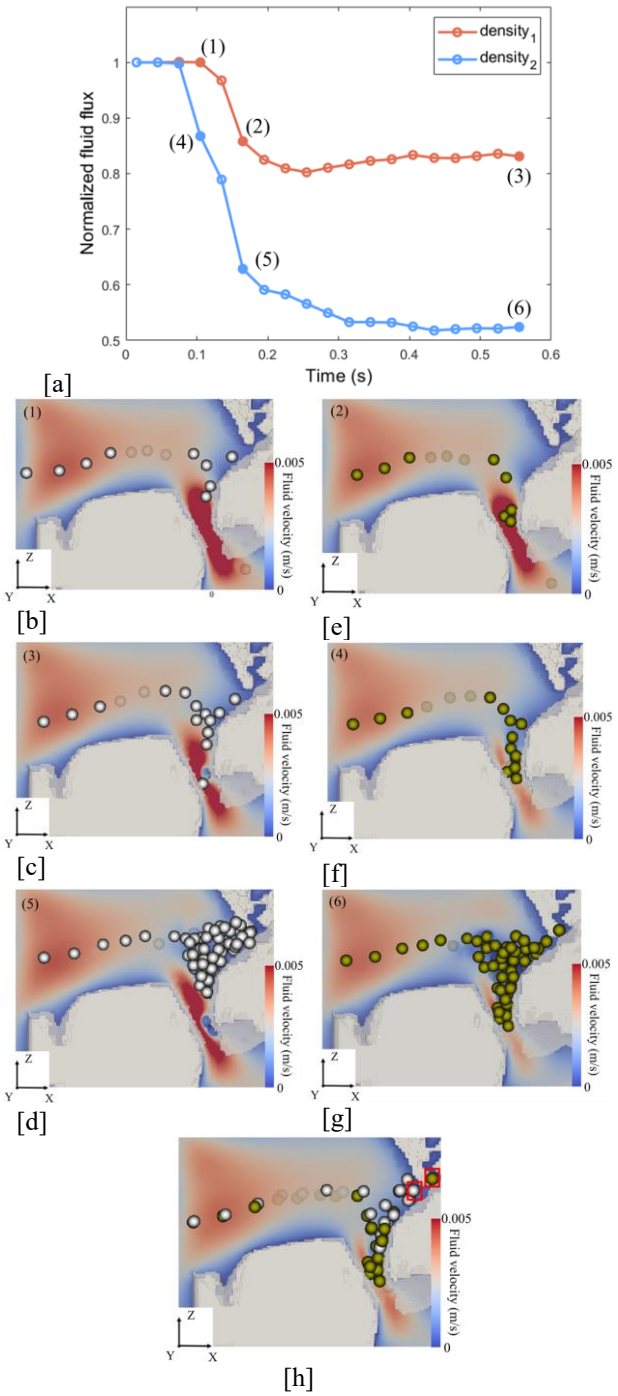

Fig. 8. [a] Temporal evolution of fluid flux in the gravitationally downward throat (see Fig. 6) for the two cases involving fines of differing densities. The fluid flux is normalized to the initial flux prior to the injection of fines. The configuration of fines accumulation and the local fluid velocity field are explored at the specific simulated times denoted by the solid data points. [b]-[g] fines configurations and corresponding velocity fields for the times corresponding to the solid datapoints of [a]; [b], [c] and [d] are the snapshot of locations of the neutrally buoyant fines at the simulated time of 0.1 s, 0.16 s, and 0.55 s, respectively, each shown with the local fluid velocity field. [e], [f] and [g] are the snapshot of locations of the dense fines at the simulated time of 0.1 s, 0.16 s, and 0.55 s, respectively, each shown with the local fluid velocity field. [h] Comparison of configuration between neutrally buoyant and denser fines at 0.185 s. The red frame marks a pair of concurrent fines.

velocity distribution. Fig. 8a demonstrates the decrease of fluid flux through the objective throat in both filtration cases, while a more pronounced reduction is observed in the case involving the fines with higher density. Initially, the neutrally buoyant fines attach at the throat's entrance, yielding a negligible impact on the throat's flux (Fig. 8b). At a simulated time of 0.16 s, as the injection of fines continues, they progressively accumulate at the throat's entrance, and a couple of fines intrude the throat, which results in 15% flux reduction (Fig. 8c). The neutrally buoyant fines continue to accumulate at the rear of the growing aggregate above the throat, instead of infiltrating into the throat. During this period, the flux exhibits a minimal decline, which can be attributed to the confinement of flow space at the throat's entrance due to the accumulation of fines, along with the settlement of the fines within the throat. Fig. 8d demonstrates that the development of fines cluster alters the initial flow pattern, causing an earlier bifurcation of the fluid flow. The cluster development reshapes the fluid field and causes a slight flux increase (Fig. 8a(2) to Fig. 8a(3)).

In comparison, denser fines initially invade and accumulate within the throat, resulting in an approximate 13% flux reduction (Fig. 8e). The cluster of retained fines continues to grow within the throat. As shown in Fig. 8f, the growth of the retained fines cluster significantly enhances flow resistance and dramatically decreases fluid velocity within the throat, correlating with a flux reduction to 63% of its original level at 0.16s. However, Fig. 8g reveals significant cluster growth above the throat, while growth within the throat remains limited. Consequently, the fluid flux decreases more slowly during this period. This can be attributed to the decrease in fluid flux into the downward throat, which weakens the downward component of the hydraulic force acting on the subsequently approaching fines, thereby limiting their entry into the throat. As a result, the hydraulic force fails to drive the fines into the downward throat, leading the denser fines to choose the upward pathway instead. Fig. 8h demonstrates that a denser particle is retained within the upward channel, and displays an elevated retention position in the gravity direction and a more extended transport distance along the flow direction.

It should be noted that the peak of the distribution appears near zero both in the Z direction and X direction. This indicates that in the majority of concurrent particle pairs, the final retention positions of the two fines with different densities are close to each other, signifying no pronounced trajectory deviations between them. Given the favorable attachment conditions employed in our simulation, alongside the intricate pore geometry of sandstone, fines tend to experience collisions and subsequent capture by grain surfaces shortly after their ingress into the porous matrix. The gravitational forces acting on the denser fines appear insufficient to cause significant deviations from the prescribed streamlines within the limited travel time, reinforcing the notion that fluid flow remains the dominant factor in fines transport.

4 Conclusion

In this study, we explore the impact of gravity on transport and retention of fine particles within Bentheimer sandstone by employing the CFD-DEM approach with a complete force set. The geometrical structures of the simulated porous media are generated from a 3D micro-CT image. We employ an octree mesh technique that adaptively refines the CFD cells populated by fines to the desired resolution to significantly reduce the overall number of cells in fluid flow simulations, thereby reducing the computational cost. Furthermore, the trajectories of fines are tracked and pairwise comparison of fines motion and retention for fines with same starting positions were utilized. Fine transport simulations are conducted with two study cases with various fines densities. In contrast to neutrally buoyant fines, the denser fines exhibit a distribution leaning towards the bottom and inlet surface of the sample, which suggests that gravity promotes the transport of fines in the direction of its pull, while restricting the transport distance along the flow direction.

The distribution of trajectory deviations among fines of varying densities reveals that a considerable portion (approximately 40%) of the denser fines exhibit limited transport in the direction of gravity and enhanced transport along the flow direction. The observations of fines transport in particular pores and throats indicate that this unexpected transport behavior is caused by two mechanisms due to the complex flow domain with sandstone. Firstly, gravity assists denser particles to pass through the downward throat, thereby resulting in more extensive distances. The second mechanism is that the denser fines invade the downward throat and subsequently clog the throat. The clogging structure changes the fluid flow flux in the pathways. This clogging alters the fluid flux in the clogged throat and changes fluid pathways, which in turn modifies the trajectory of incoming fines and can potentially extend their transport distance. The proposed model can be customized to accommodate the porous media when the corresponding 3D images are available.

In this study, a favorable condition for fines attachment is employed, which constrains the deviations between the trajectories of neutrally buoyant and denser fines. In future work we will consider a wider range of fines densities, along with the incorporation of varying flow rates and ionic strengths to provide a more comprehensive understanding of gravity effects on fines transport within sandstones and quantifying the relative impact of the different parameters on fines retention.

References

[1] G. Tang, N.R. Morrow, J. Pet. Sci. Eng., **24**, 99 (1999)

[2] M.M. Sharma, Y.C. Yortsos, AIChE J., **33** (1987)

[3] Q. Xie, A. Saeedi, C.D. Piane, L. Esteban, P.V. Brady, Int. J. Greenh. Gas Control., **65** (2017)

[4] E.B. Janetti, I. Dror, M. Riva, A. Guadagnini, X. Sanchez-Vila, B. Berkowitz, Transp Porous Med, **97**, 295 (2013)

[5] S.K. Ngueleu, P. Grathwohl, O.A. Cirpka, J. Contam. Hydrol., **162**, 47 (2014)

[6] N. Saleh, T. Phenrat, K. Sirk, B. Dufour, J. Ok, T. Sarbu, K. Matyjaszewski, Nano letters, **5**, 2489 (2005)

[7] R.W. Harvey, S.P. Garabedian, Environ Sci Technol, **25**, 178 (991)

[8] S.C. James, T.K. Bilezikjian, C.V. Chrysikopoulos, Stoch Environ Res Risk Assess, **19**, 266 (2005)

[9] S.A. Bradford, S.R. Yates, M. Bettahar, J. Simunek, Water Resour Res, **38**, 12 (2002)

[10] W.P. Johnson, X. Li, G. Yal, Environ. Sci. Technol., **4**, 1279 (2007)

[11] S. Liu, I. Shikhov, Y. Cui, C. Arns, Geoenergy Sci and Eng, **227**, 211772 (2023)

[12] S. Torkzaban, S.A. Bradford, Water research, **88**, 274 (2015)

[13] C. Shen, V. Lazouskaya, H. Zhang, F. Wang, B. Li, Y. Huang, Physicochem. Eng. Aspects, **410**, 98 (2012)

[14] S.A. Bradford, S. Torkzaban, H. Kim, J. Simunek, Water Resour Res, **48** (2012)

[15] S.A. Bradford, S. Torkzaban, S.L. Walker, Water research, **41**, 3012 (2007)

[16] P. Bedrikovetsky, A. Zeinijahromi, F.D. Siqueira, C.A. Furtado, A.L.S. de Souza, Transp Porous Media, **91**, 173 (2012)

[17] R.A.J. Vaidyanathan, C. Tien, Chem Eng Commun, **81**, 123 (1989)

[18] G. Chen, Y. Hong, S.L. Walker, Langmuir, **26**, 314 (2010)

[19] C. Chrysikopoulos, V.I. Syngouna, Environ. Sci. Technol.,**48**, 6805 (2014)

[20] S. Torkzaban, S. Bradford, J. Contam. Hydrol., **181**, 161 (2015)

[21] Q. Liu, B. Zhao, J.C. Santamarina, Wiley Online Library, **124**, 9495 (2019)

[22] J. Wan, T. Tokunaga, C. Tsang, Wiley Online Library, **31**, 1627 (1995)

[23] S. Berg and J. Van Wunnik, Transp Porous Media,**117**,229 (2017)

[24] H.J. Khan, M.S. Mirabolghasemi, H. Yang , M. Prodanović, D.A. DiCarlo, M.T. Balhoff, J. Pet. Sci. Eng., **158**, 293 (2017)

[25] A. Elrahmani, R.I. Ai-Raoush, H. Abugazia, T. Seers, Powder Technology, **398** (2022)

[26] M.S. Kermani, S Jafari, M. Rahnama, A. Raoof, Adv. Water Resour., **144** (2020)

[27] G. Gerber, M. Bensouda, D.A. Weitz, P. Coussot, Phys Rev Lett, **123** (2019)

[28] O.R. Walton, R.L. Braun, J Rheol, **30**, 949 (1986)

[29] S. Safran, *Statistical thermodynamics of surfaces, interfaces, and membranes* (2018)

[30] H.C Hamaker, *physica*, **4** (1937)

[31] C. Kloss, C. Goniva, A. Hager, S. Amberger, S. Pirker, Prog. Comput. Fluid Dyn., **12**, 140 (2012)

[32] A. Sheppard, R.M. Sok, H. Averdunk, Phys. A: Stat. Mech. Appl., **339**, 145 (2004)

[33] H.G. Weller, G. Tabor, H. Jasak, C. Fureby, Computers in physics, **12**, 620 (1998)
[34] P. Soille, *Morphological image analysis: principles and applications* (1999)
[35] G.R. McNamara and G. Zanetti, Phys Rev Lett, **61**, 2332 (1988)
[36] N.S. Martys, J.G. Hagedorn, Mater Struct, **35**, 650 (2002)
[37] D. Meagher, *Octree Encoding: A New Technique for the Representation, Manipulation and Display of Arbitrary 3-D Objects by Computer* (1980)
[38] A. Hager, C. Kloss, S. Pirker, C. Goniva, J. Comput. Multiph. Flows, **6**, 13 (2014)
[39] N. Tufenkji, M. Elimelech, Langmuir, **21**, 841 (2005)
[40] P. Leroy, A. Maineult, S. Li, J. Vinogradov, Colloids Surf A Physicochem Eng Asp, **650** (2022)
[41] S.C. James. C.V Chrysikopoulos, J Colloid Interface Sci, **270**, 250 (2004)